Figure Legends

1. The geometry of the model RyR pore. In the experiments and calculations, the lumen of the sarcoplasmic reticulum (SR) is electrically grounded. The circle around each labeled amino acid in meant to illustrate the range of the motion of the terminal carboxyl group. Aspartates (solid circles) are given a radius of 5 Å and glutamates (dashed circles) 7 Å. Only the amino acids of one of the four identical RyR subunits is shown. Asp-4945, Asp-4938, Asp-4899, Glu-4900, and Glu-4902 are the only amino acids explicitly modeled in the theory. The GGGIG sequence (4894-4898 in the numbering) at the cytosolic end of the selectivity filter is only a reference point for readers familiar with the RyR sequence.
2. Experimental verification of the AMFE predicted by the theory. The lines are the theory and the symbols are the experimental data with standard error bars and the number of experiments in parentheses. The solid line and symbols are the addition of Ca^{2+} to Na^{+} and the dashed line and open symbols are the addition of Ca^{2+} to Cs^{+}. In all cases, the monovalent-chloride concentration was 150 mM in both cytosolic and lumenal baths and the indicated amount Ca^{2+} was added to the lumenal bath. The current at -20 mV is shown.
3. The partitioning coefficient of K^{+} (panel A) and Ca^{2+} (panel B) plotted logarithmically. $[K^{+}]$ = 150 mM and the indicated $[Ca^{2+}]$ is in both baths.
4. The electrostatic component of partitioning $z_i e\phi(x)/kT$ of K^{+} (panel A) and Ca^{2+} (panel B) in the pore. $[K^{+}]$ = 150 mM and the indicated $[Ca^{2+}]$ is in both baths.
5. The screening component of partitioning $\Delta\mu_i^{SC}(x)/kT$ of K^{+} (solid lines) and Ca^{2+} (dashed lines) in the pore. $[K^{+}]$ = 150 mM and $[Ca^{2+}]$ is changed from 1 μM to 50 mM. Because the curves are so close together $[Ca^{2+}]$ is not indicated.
6. The excluded-volume (hard-sphere) component of partitioning $\Delta\mu_i^{HS}(x)/kT$ of K^{+} (solid lines) and Ca^{2+} (dashed lines) in the pore. $[K^{+}]$ = 150 mM and $[Ca^{2+}]$ is changed from 1 μM to 50 mM. Because the curves are so close together $[Ca^{2+}]$ is not indicated.
7. Components of the binding selectivity from Eq. (6) in the selectivity filter (x = 20 Å in Fig. 1 that shows the geometry of the pore). $[K^{+}]$ = 150 mM and the indicated $[Ca^{2+}]$ is in both baths. The horizontal-hatched bar is the number advantage, the diagonal-hatched bar is the mean electrostatic advantage, the cross-hatched bar is the screening advantage, and the solid bar is the excluded-volume advantage. The horizontal line is the binding selectivity of Eq. (6) (i.e., the sum of all the terms). A positive term favors the binding of Ca^{2+} while a negative term favors K^{+}.
8. Concentration profiles in the pore of the monovalent cation (panel A) and Ca^{2+} (panel B). For each indicated monovalent cation X^{+}, $[X^{+}]$ = 150 mM and $[Ca^{2+}]$ = 1 mM in both baths.
9. Components of the binding selectivity from Eq. (6) in the selectivity filter (x = 20 Å in Fig. 1 that shows the geometry of the pore). For each indicated monovalent cation X^{+}, $[X^{+}]$ = 150 mM and $[Ca^{2+}]$ = 1 mM in both baths. Ion diameters: Li^{+} 1.33 Å; Na^{+} 2.00 Å; K^{+} 2.76 Å; Cs^{+} 3.42 Å. The horizontal-hatched bar is the number advantage, the diagonal-hatched bar is the mean electrostatic advantage,

the cross-hatched bar is the screening advantage, and the solid bar is the excluded-volume advantage. The horizontal line is the binding selectivity of Eq. (6) (i.e., the sum of all the terms). A positive term favors the binding of Ca^{2+} while a negative term favors K^+.

10. Concentration profiles in the pore of K^+ (panel A) and Ca^{2+} (panel B) for the native (WT) channel (solid line) and the mutation D4899N (dashed line). $[K^+]$ = 150 mM and $[Ca^{2+}]$ = 1 mM in both baths. In the model, the mutation is created by "turning off" the charge on the four Asp-4899. The mutation site is the region from which the charge on the four Asp-4899 has been removed.
11. Concentration profiles in the pore of K^+ (panel A) and Ca^{2+} (panel B) for the native (WT) channel (solid line) and the mutation D4938N (dashed line). $[K^+]$ = 150 mM and $[Ca^{2+}]$ = 1 mM in both baths. In the model, the mutation is created by "turning off" the charge on the four Asp-4938. The mutation site is the region from which the charge on the four Asp-4938 has been removed.
12. Profiles of the binding selectivity from Eq. (6) (panel A) and its components (excluded volume, panel B; mean electrostatic, panel C; screening, panel D) for the native (WT) channel (solid line) and the mutation D4899N (dashed line). The conditions are those described in Fig. 9.
13. Profiles of the binding selectivity from Eq. (6) (panel A) and its components (excluded volume, panel B; mean electrostatic, panel C; screening, panel D) for the native (WT) channel (solid line) and the mutation D4938N (dashed line). The conditions are those described in Fig. 10.
14. Current/voltage curves in KCl (A-H). (I) The conductance at reversal potential with cytosolic $[K^+]$ is held at 250 mM and lumenal $[K^+]$ is varied. For both experiment and theory the current/voltage was fitted with a line and the slope is plotted. In this and the following figures, concentrations are listed as cytosolic | lumenal. The solid lines are the model and symbols are the experimental data.
15. Current/voltage curves of (A) the D4899N (■) and E4900Q (□) mutants and (B) the D4938N mutant in 250 mM symmetric KCl.
16. Current/voltage curves in LiCl. The dashed line is the model result for 250 mM cytosolic and 25 mM lumenal bath concentrations (Δ).
17. Current/voltage curves in NaCl.
18. Current/voltage curves in RbCl.
19. Current/voltage curves in CsCl.
20. Mole fraction experiments at 250 mM total cation concentration in symmetric solutions. (A) NaCl and CsCl mixtures. The experimental point at mole fraction 0.6 is statistically significantly different than the point at mole fraction 1 ($p < 0.05$). (B) LiCl and KCl mixtures.
21. Current/voltage curves in bi-ionic conditions.
22. Current/voltage curves with divalent and monovalent cations. (A) KCl and $CaCl_2$. (B) NaCl and $CaCl_2$. (C) CsCl and $CaCl_2$. (D) KCl and $MgCl_2$. In both baths are 250 mM monovant-Cl and in the lumenal bath is 5 mM (■), 10 mM (□), and 50 mM (▲) divalent-Cl_2 or the baths contain 250 mM cytosolic monovant-Cl and 25 mM lumenal divalent-Cl_2 (Δ). Current/voltage curves of (E) the D4899N (■) and E4900Q (□) mutants and (F) the D4938N mutant in 250 mM symmetric KCl and 10 mM lumenal $CaCl_2$.

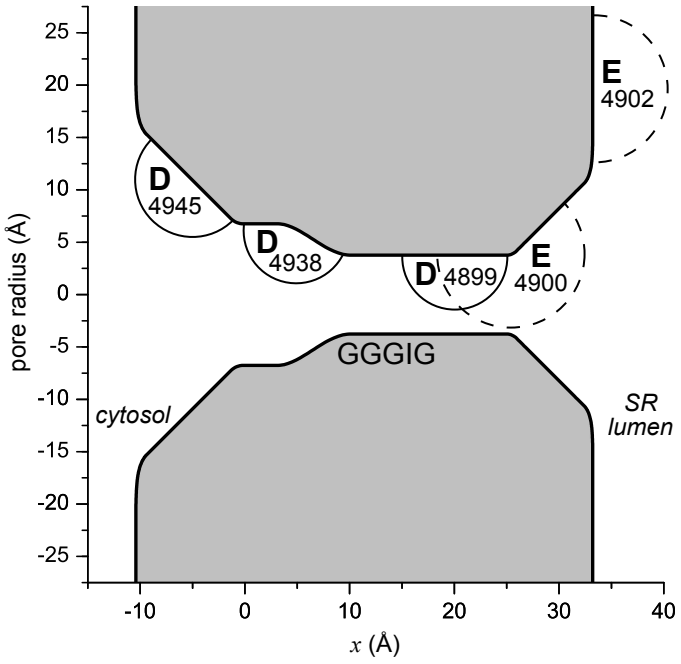
E
4902
D
4945
D
4938
D
4899
E
4900
GGGIG
cytosol
SR
lumen
pore radius (Å)
x (Å)
25
20
15
10
5
0
-5
-10
-15
-20
-25
-10
0
10
20
30
40

Fig. 1

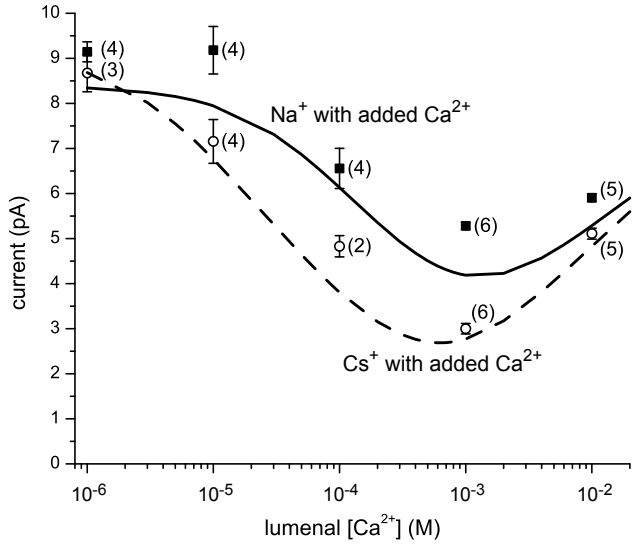
current (pA)
lumenal [Ca2+] (M)
Na+ with added Ca2+
Cs+ with added Ca2+
(4)
(3)
(4)
(4)
(4)
(2)
(6)
(6)
(5)
(5)

Fig. 2

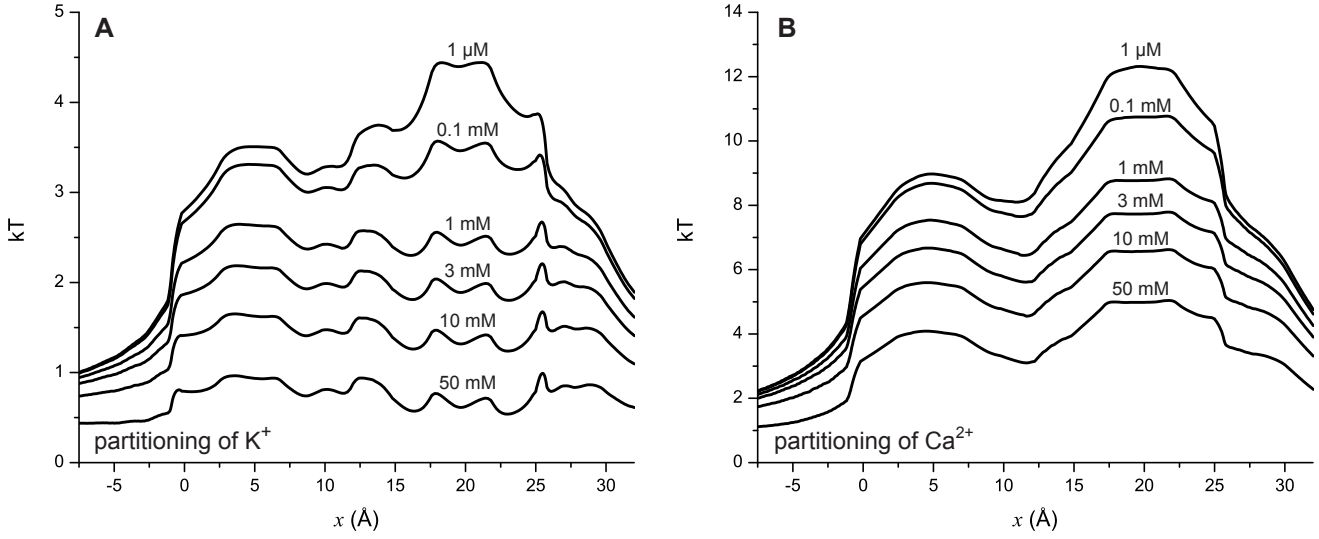
A
1 μM
0.1 mM
1 mM
3 mM
10 mM
50 mM
partitioning of K+
kT
x (Å)
B
1 μM
0.1 mM
1 mM
3 mM
10 mM
50 mM
partitioning of Ca2+
kT
x (Å)

Fig. 3

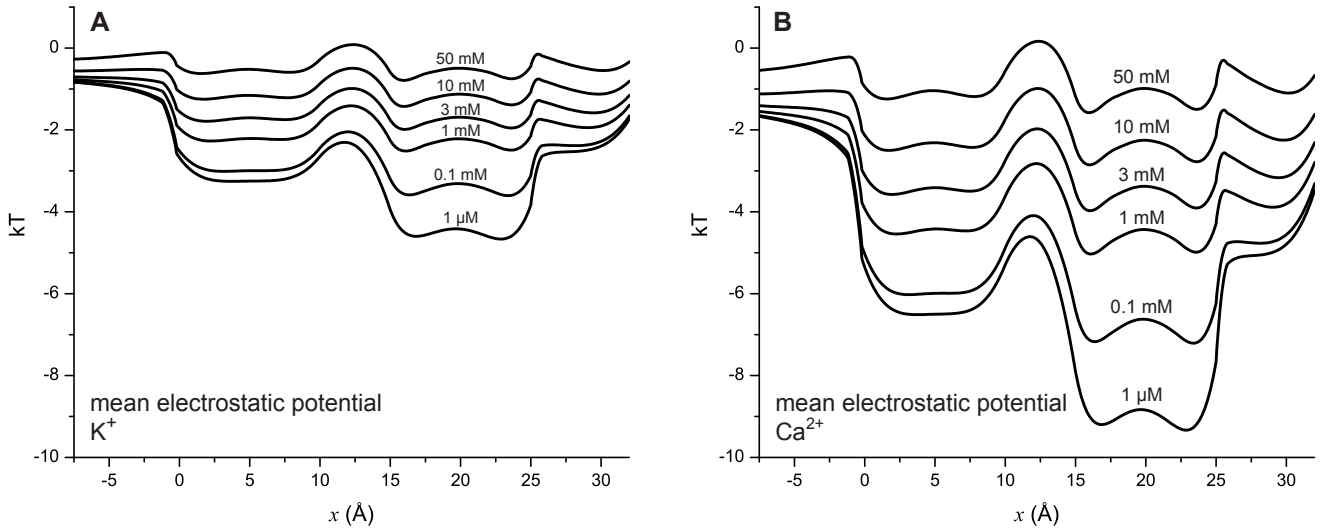
A
50 mM
10 mM
3 mM
1 mM
0.1 mM
1 μM
mean electrostatic potential
K+
kT
x (Å)
B
50 mM
10 mM
3 mM
1 mM
0.1 mM
1 μM
mean electrostatic potential
Ca2+
kT
x (Å)

Fig. 4

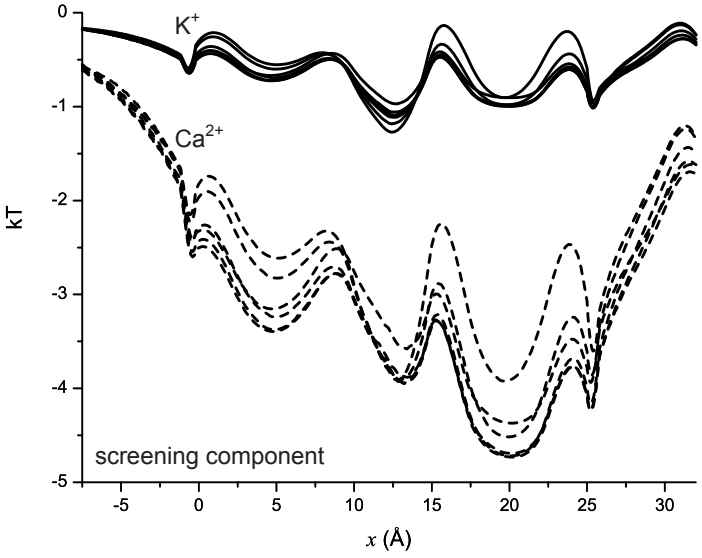

Fig. 5

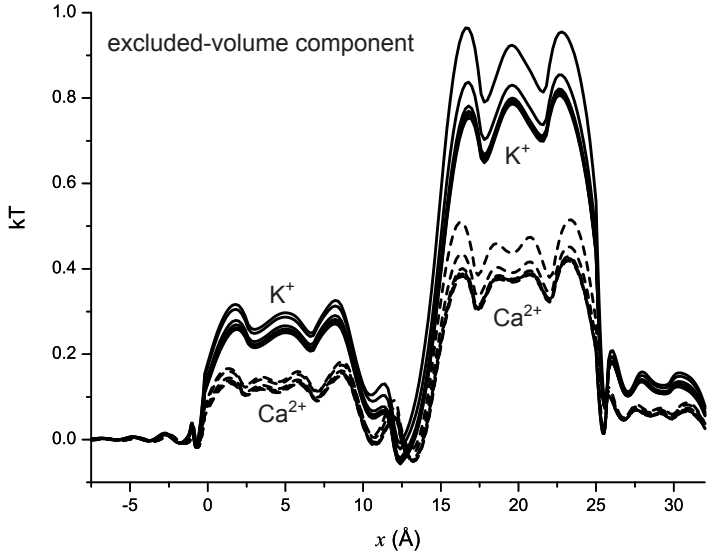
excluded-volume component
kT
x (Å)
K+
Ca2+
K+
Ca2+
1.0
0.8
0.6
0.4
0.2
0.0
-5
0
5
10
15
20
25
30

Fig. 6

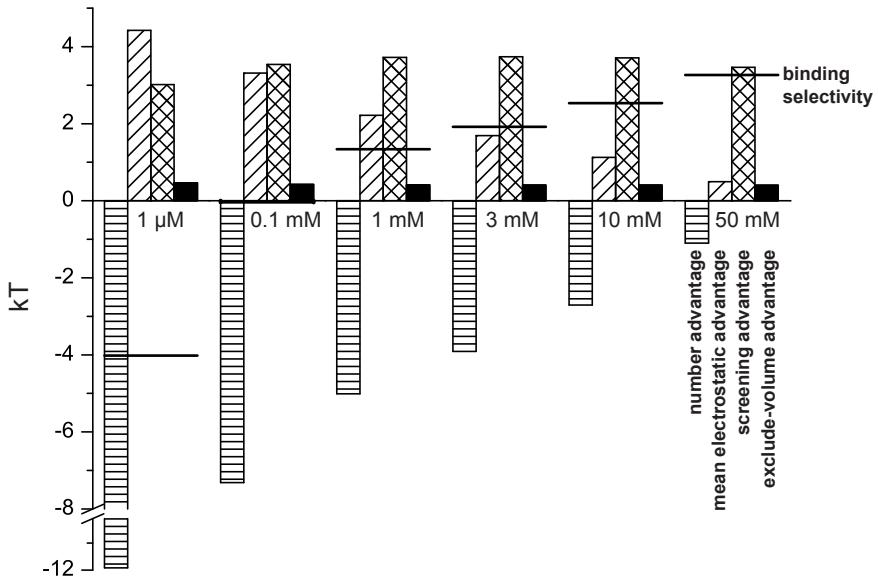
4
2
0
-2
-4
-6
-8
-12
kT
1 μM
0.1 mM
1 mM
3 mM
10 mM
50 mM
binding selectivity
number advantage
mean electrostatic advantage
screening advantage
exclude-volume advantage

Fig. 7

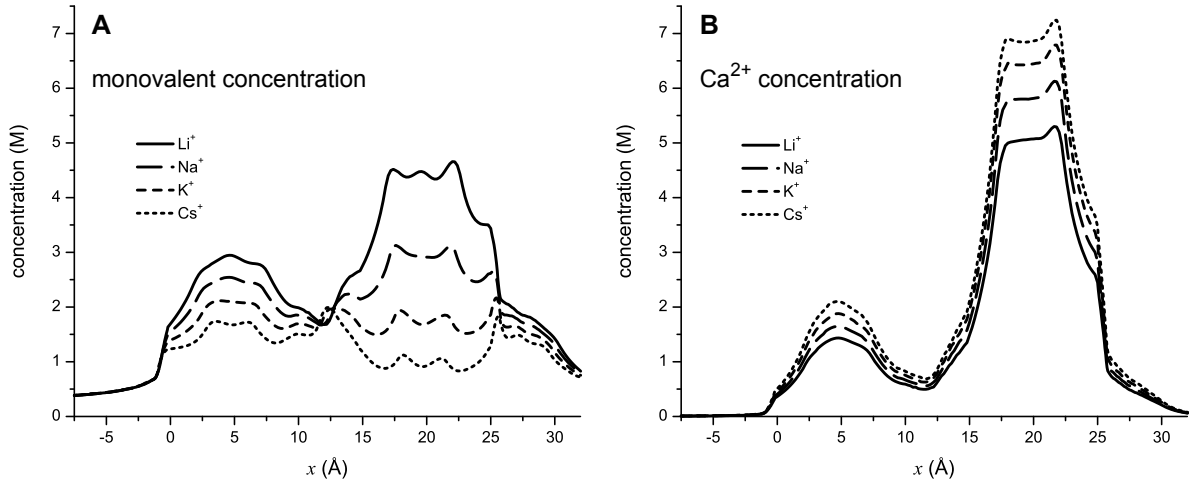
A
monovalent concentration
Li+
Na+
K+
Cs+
concentration (M)
x (Å)
B
Ca2+ concentration
Li+
Na+
K+
Cs+
concentration (M)
x (Å)

Fig. 8

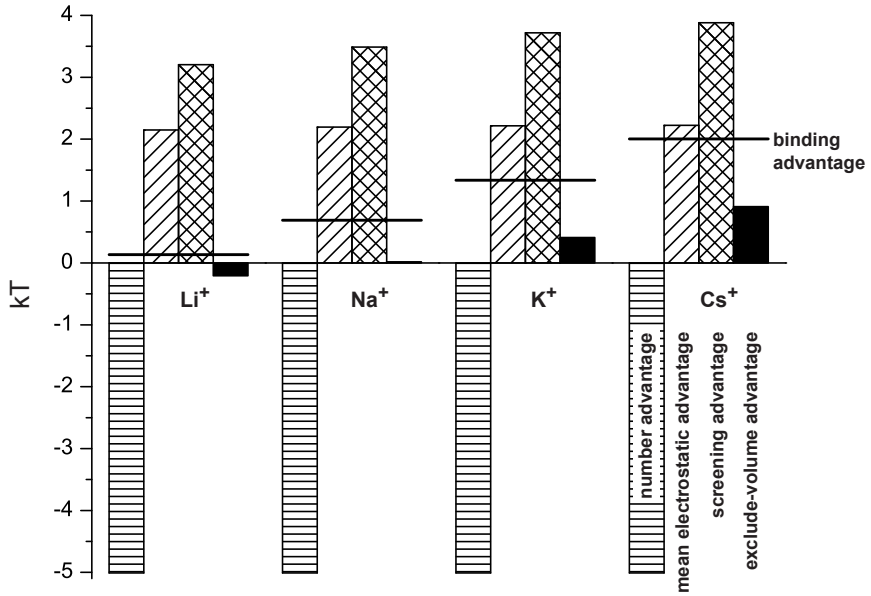
4
3
2
1
0
-1
-2
-3
-4
-5
kT
Li+
Na+
K+
Cs+
binding advantage
number advantage
mean electrostatic advantage
screening advantage
exclude-volume advantage

Fig. 9

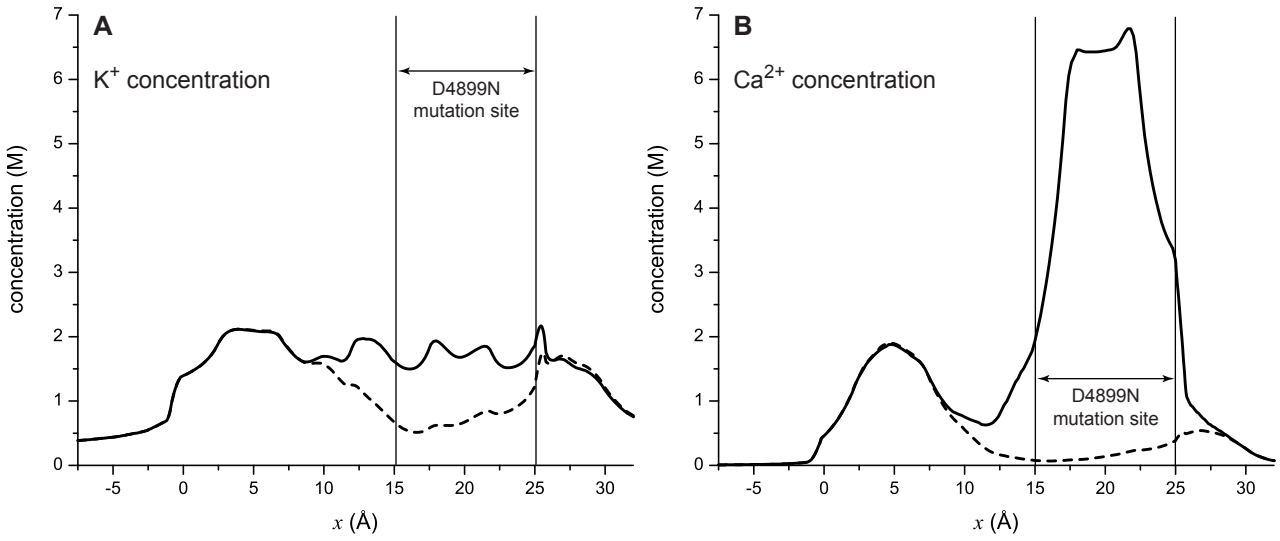
A
K+ concentration
D4899N
mutation site
concentration (M)
x (Å)
B
Ca2+ concentration
D4899N
mutation site
concentration (M)
x (Å)

Fig. 10

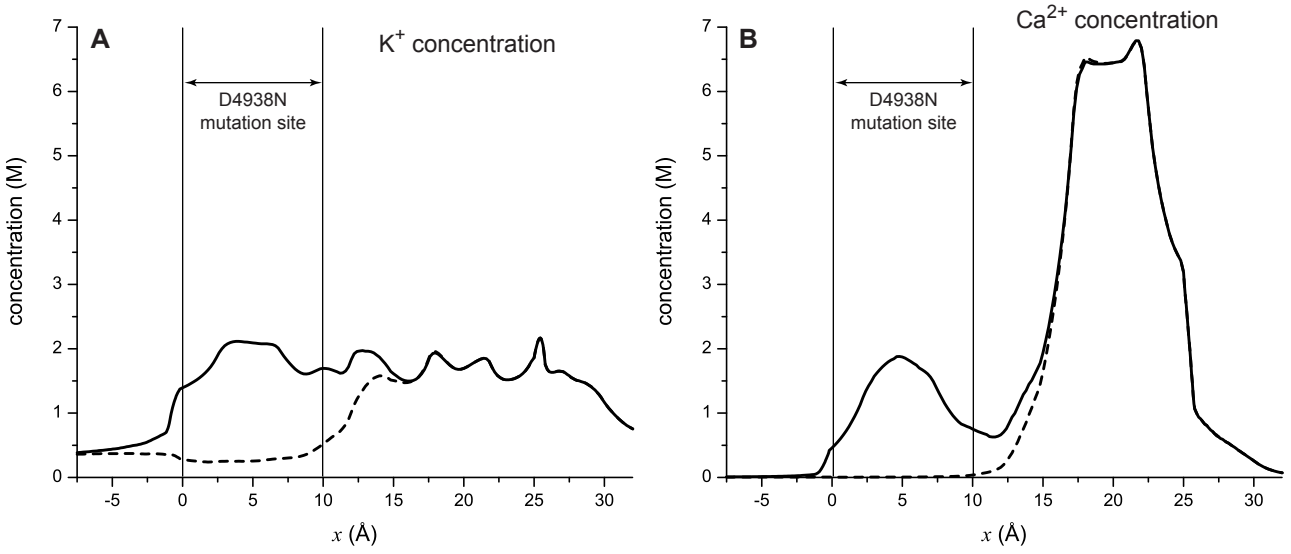
A
K+ concentration
D4938N
mutation site
concentration (M)
x (Å)
B
Ca2+ concentration
D4938N
mutation site
concentration (M)
x (Å)

Fig. 11

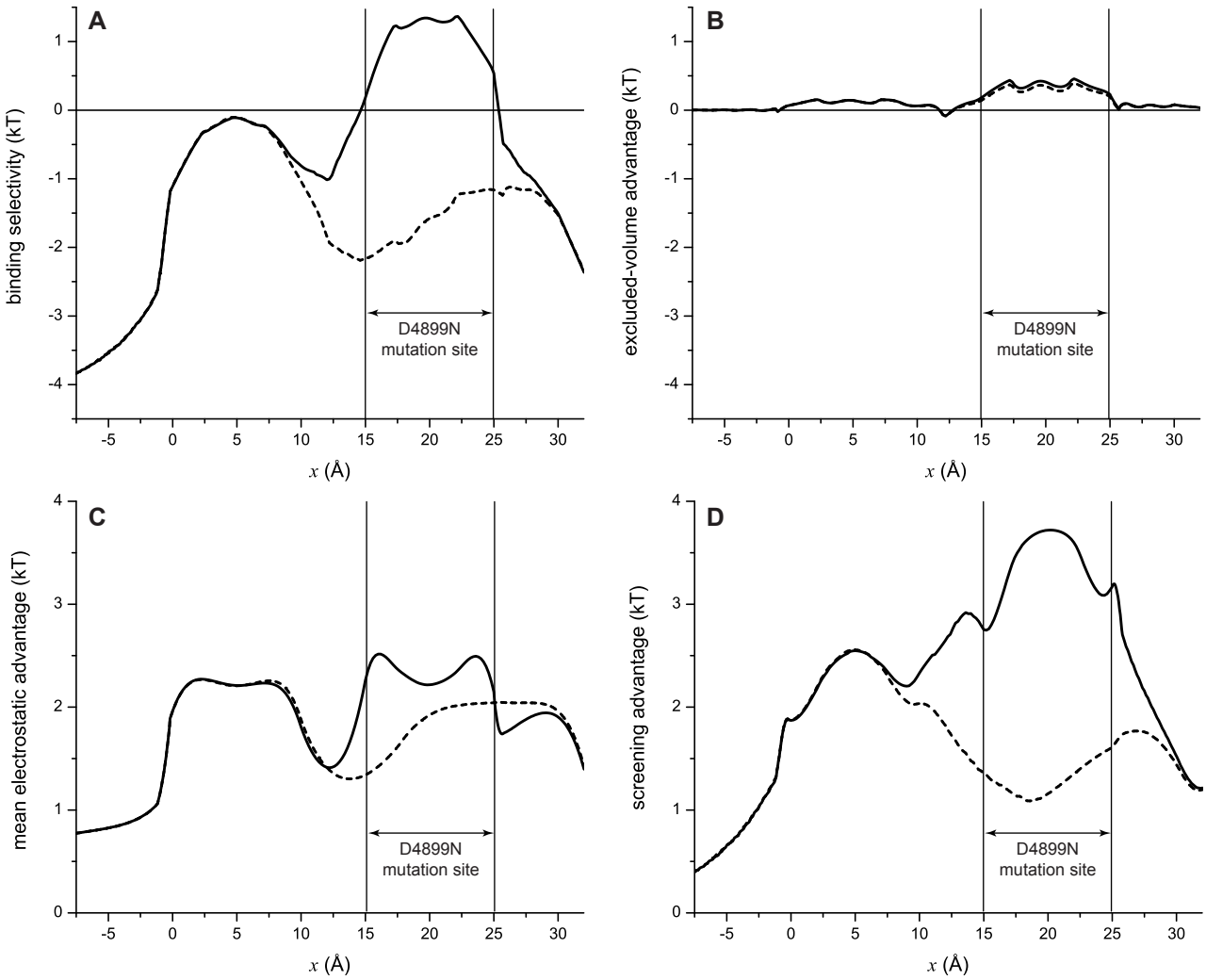
A
binding selectivity (kT)
D4899N
mutation site
x (Å)
B
excluded-volume advantage (kT)
D4899N
mutation site
x (Å)
C
mean electrostatic advantage (kT)
D4899N
mutation site
x (Å)
D
screening advantage (kT)
D4899N
mutation site
x (Å)

Fig. 12

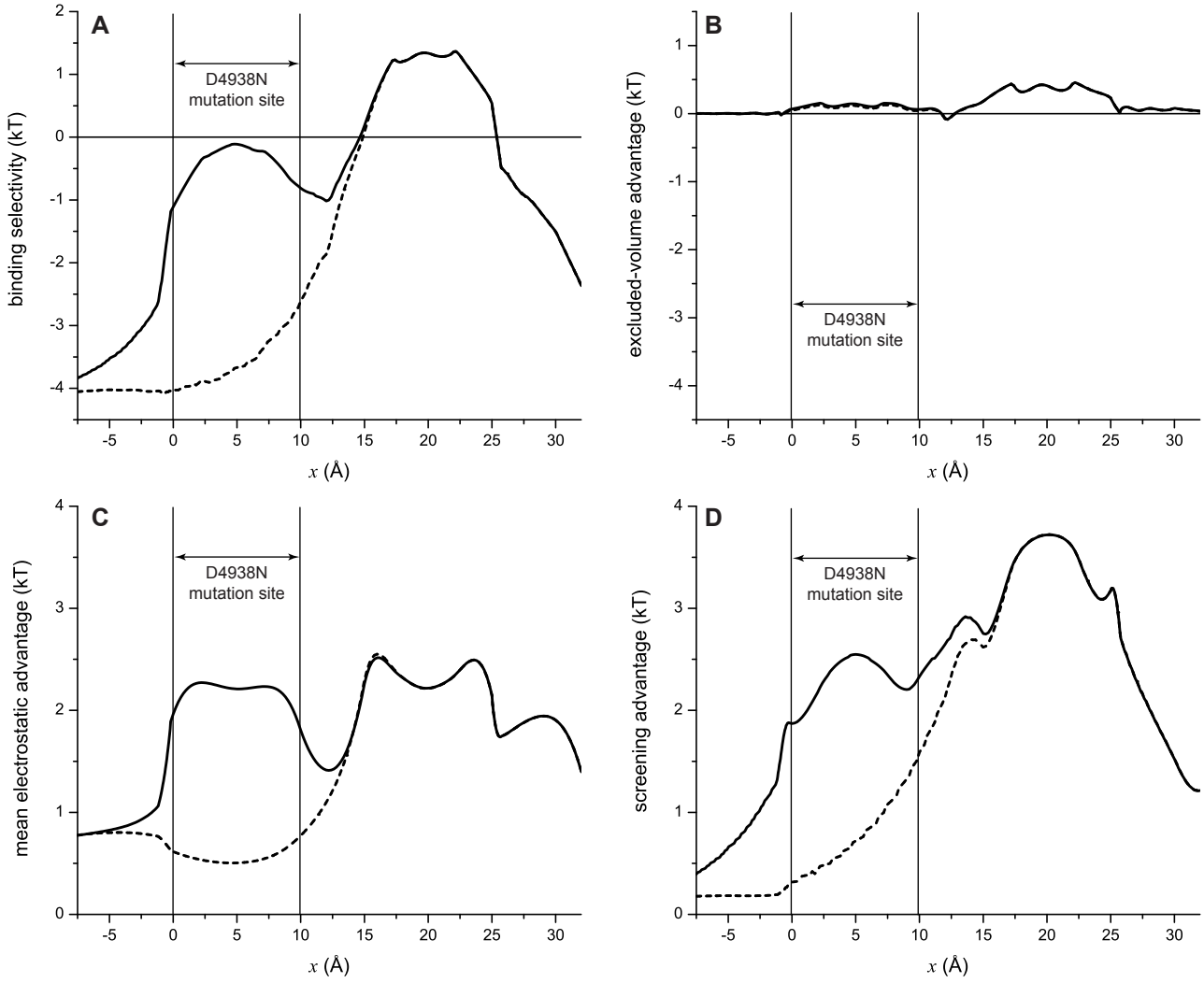
A
D4938N
mutation site
binding selectivity (kT)
x (Å)
B
D4938N
mutation site
excluded-volume advantage (kT)
x (Å)
C
D4938N
mutation site
mean electrostatic advantage (kT)
x (Å)
D
D4938N
mutation site
screening advantage (kT)
x (Å)

Fig. 13

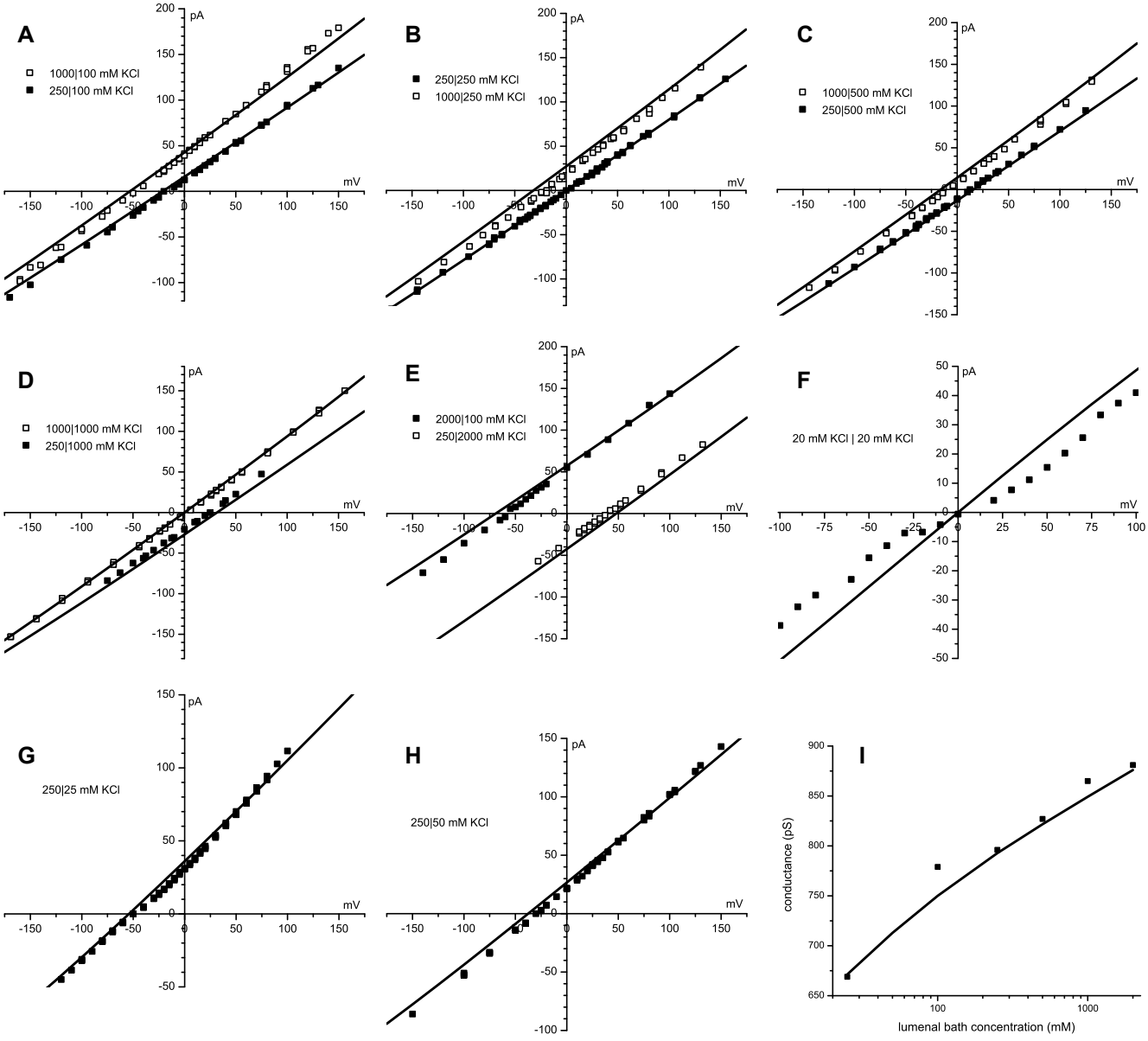
A
1000|100 mM KCl
250|100 mM KCl
B
250|250 mM KCl
1000|250 mM KCl
C
1000|500 mM KCl
250|500 mM KCl
D
1000|1000 mM KCl
250|1000 mM KCl
E
2000|100 mM KCl
250|2000 mM KCl
F
20 mM KCl | 20 mM KCl
G
250|25 mM KCl
H
250|50 mM KCl
I
conductance (pS)
lumenal bath concentration (mM)
pA
mV

Fig. 14

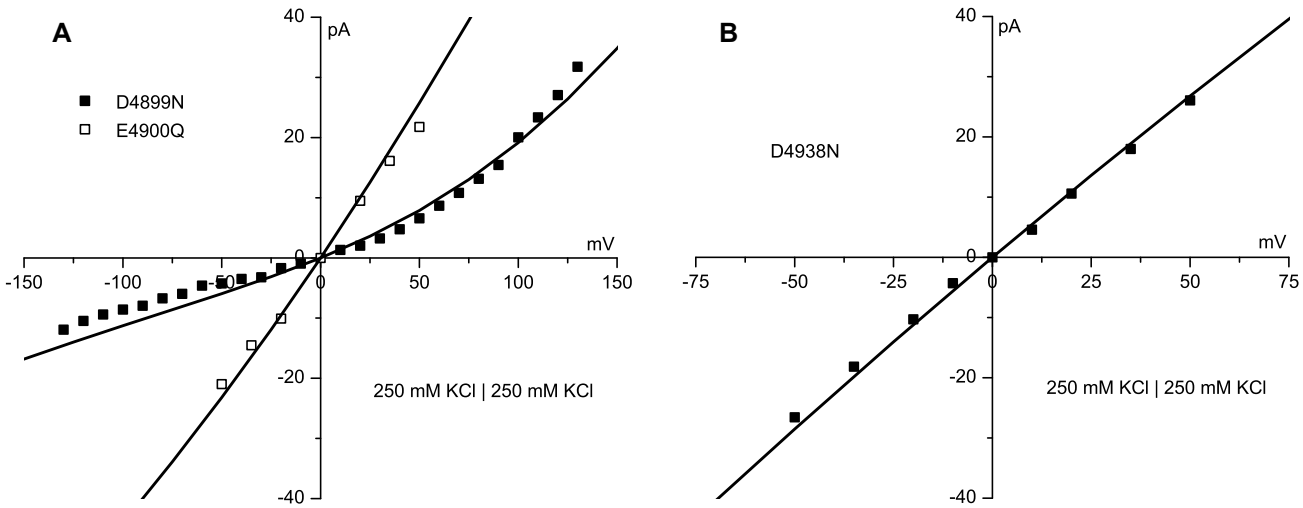
A
pA
40
20
0
-20
-40
mV
-150
-100
-50
0
50
100
150
D4899N
E4900Q
250 mM KCl | 250 mM KCl
B
pA
40
20
0
-20
-40
mV
-75
-50
-25
0
25
50
75
D4938N
250 mM KCl | 250 mM KCl

Fig. 15

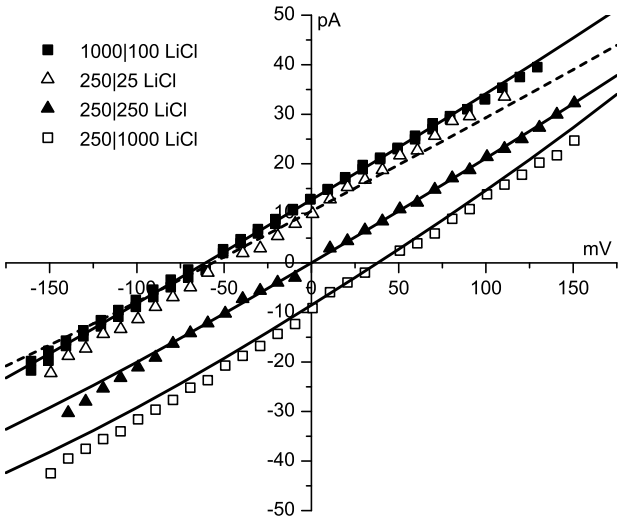
1000|100 LiCl
250|25 LiCl
250|250 LiCl
250|1000 LiCl
pA
mV
50
40
30
20
10
0
-10
-20
-30
-40
-50
-150
-100
-50
0
50
100
150

Fig. 16

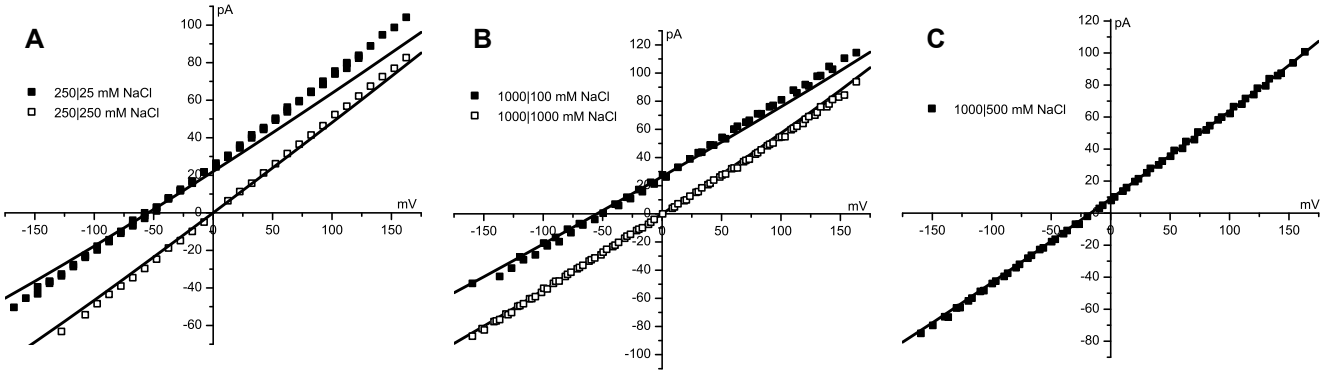
A
250|25 mM NaCl
250|250 mM NaCl
pA
mV
B
1000|100 mM NaCl
1000|1000 mM NaCl
pA
mV
C
1000|500 mM NaCl
pA
mV

Fig. 17

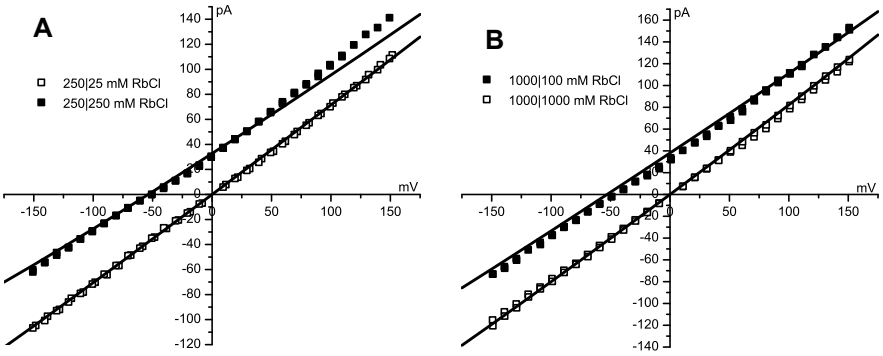
A
250|25 mM RbCl
250|250 mM RbCl
pA
mV
B
1000|100 mM RbCl
1000|1000 mM RbCl
pA
mV

Fig. 18

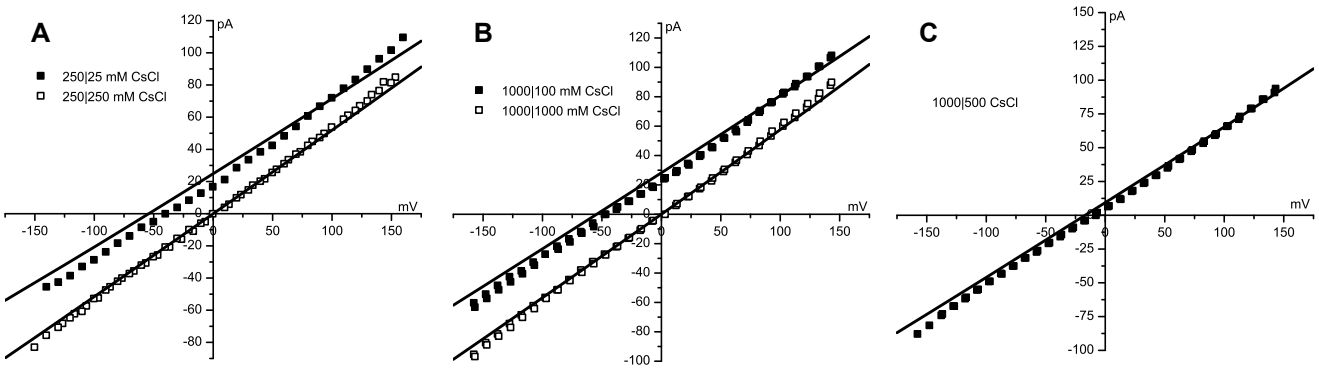
A
250|25 mM CsCl
250|250 mM CsCl
pA
mV
B
1000|100 mM CsCl
1000|1000 mM CsCl
pA
mV
C
1000|500 CsCl
pA
mV

Fig. 19

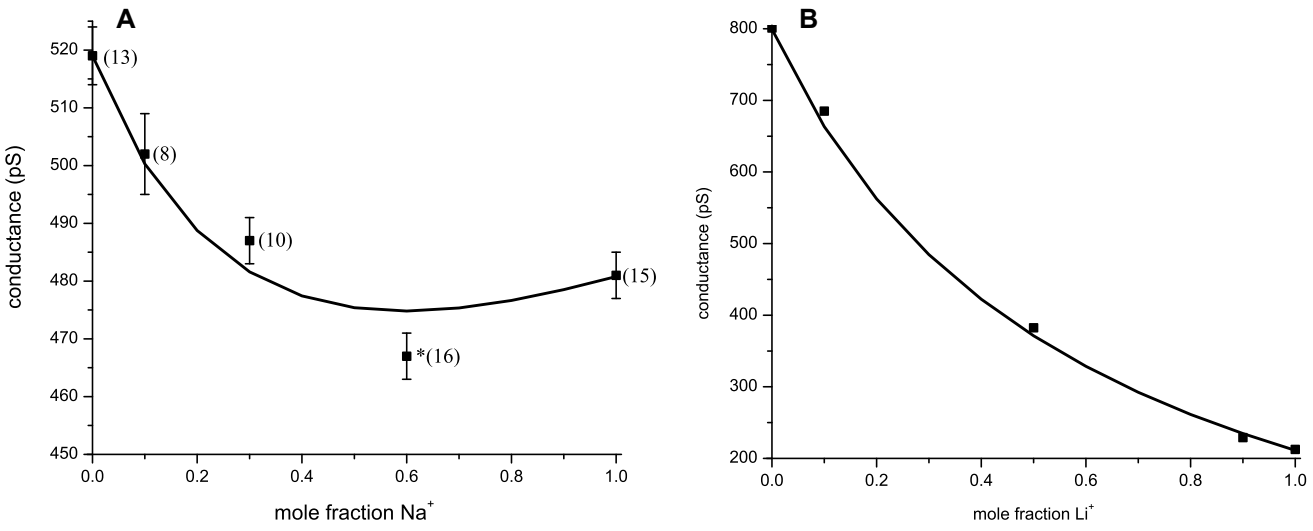
A
conductance (pS)
520
510
500
490
480
470
460
450
(13)
(8)
(10)
*(16)
(15)
0.0
0.2
0.4
0.6
0.8
1.0
mole fraction Na+
B
conductance (pS)
800
700
600
500
400
300
200
0.0
0.2
0.4
0.6
0.8
1.0
mole fraction Li+

Fig. 20

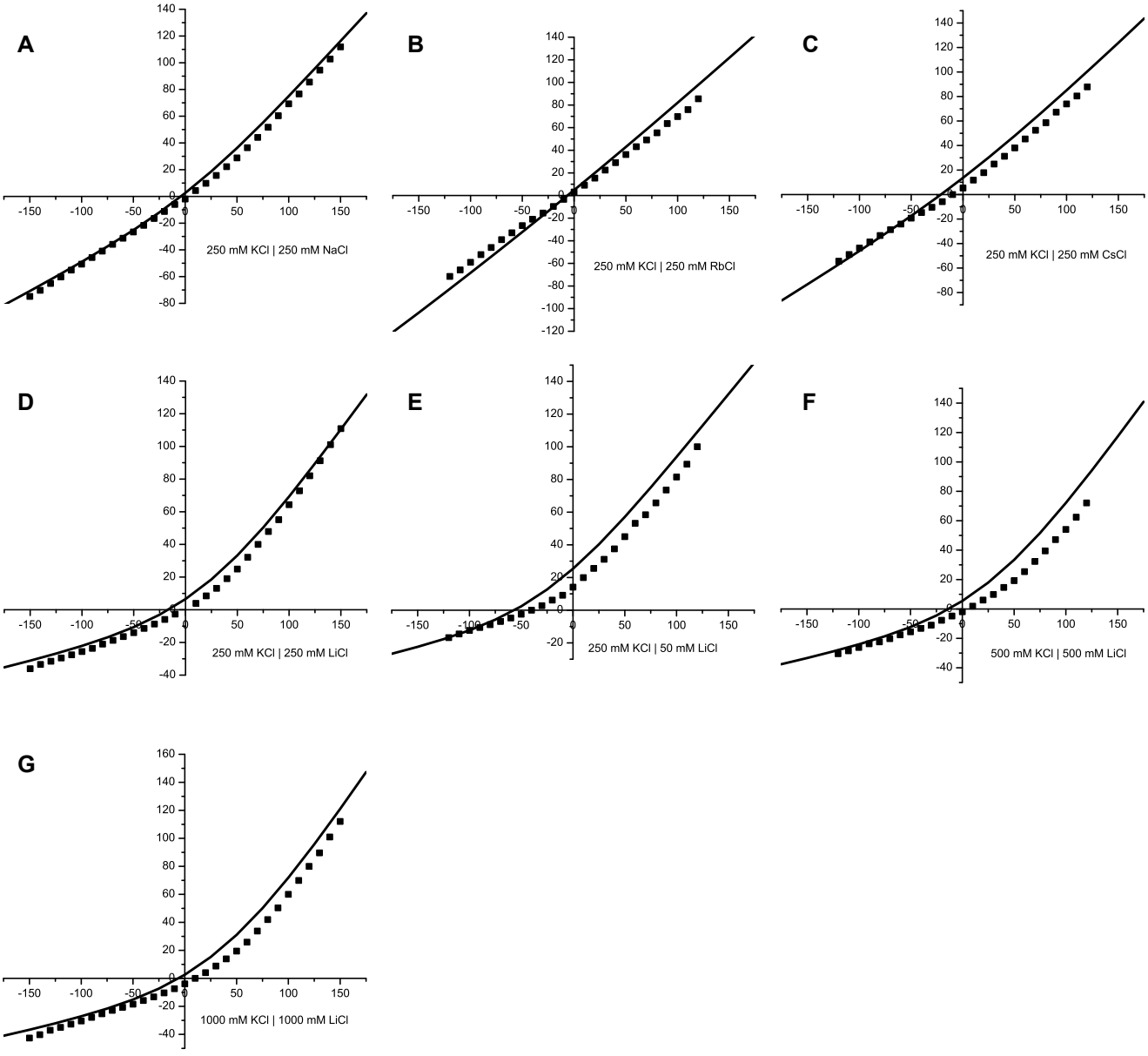
A
250 mM KCl | 250 mM NaCl
B
250 mM KCl | 250 mM RbCl
C
250 mM KCl | 250 mM CsCl
D
250 mM KCl | 250 mM LiCl
E
250 mM KCl | 50 mM LiCl
F
500 mM KCl | 500 mM LiCl
G
1000 mM KCl | 1000 mM LiCl

Fig. 21

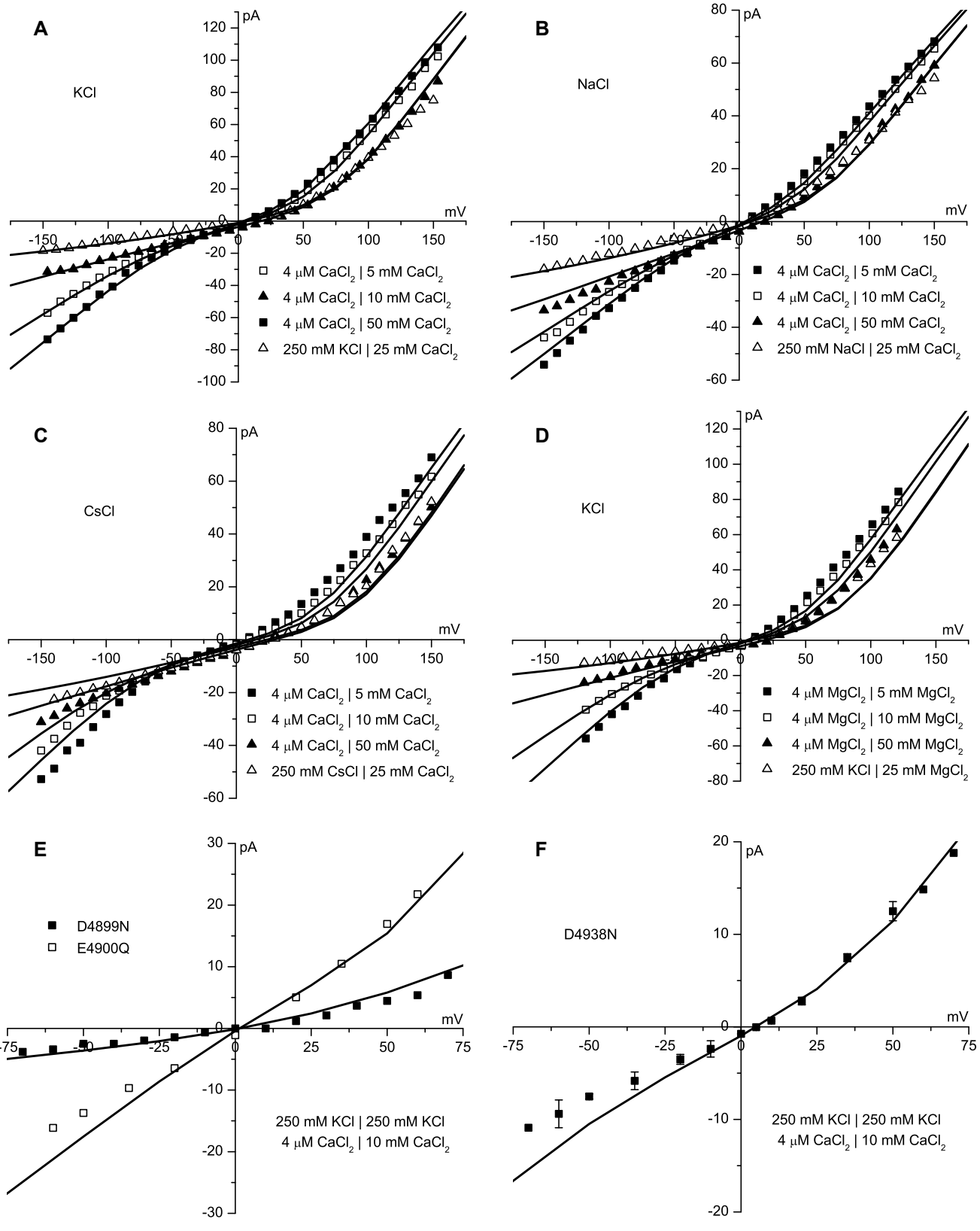
A
KCl
pA
mV
4 μM CaCl2 | 5 mM CaCl2
4 μM CaCl2 | 10 mM CaCl2
4 μM CaCl2 | 50 mM CaCl2
250 mM KCl | 25 mM CaCl2
B
NaCl
pA
mV
4 μM CaCl2 | 5 mM CaCl2
4 μM CaCl2 | 10 mM CaCl2
4 μM CaCl2 | 50 mM CaCl2
250 mM NaCl | 25 mM CaCl2
C
CsCl
pA
mV
4 μM CaCl2 | 5 mM CaCl2
4 μM CaCl2 | 10 mM CaCl2
4 μM CaCl2 | 50 mM CaCl2
250 mM CsCl | 25 mM CaCl2
D
KCl
pA
mV
4 μM MgCl2 | 5 mM MgCl2
4 μM MgCl2 | 10 mM MgCl2
4 μM MgCl2 | 50 mM MgCl2
250 mM KCl | 25 mM MgCl2
E
D4899N
E4900Q
pA
mV
250 mM KCl | 250 mM KCl
4 μM CaCl2 | 10 mM CaCl2
F
D4938N
pA
mV
250 mM KCl | 250 mM KCl
4 μM CaCl2 | 10 mM CaCl2

Fig. 22